



# Phytosynthesis, Characterization, Phenolic and Biological Evaluation of *Leptadenia pyrotechnica*-Based Zn and Fe Nanoparticles Utilizing Two Different Extraction Techniques

Rana Ahmed El-Fitiary <sup>1,2</sup>, Afra AlBlooshi<sup>1</sup>, Abdelouahid Samadi<sup>1</sup>, Mohammad A Khasawneh <sup>1</sup>

<sup>1</sup>Department of Chemistry, College of Science, United Arab Emirates University, Al Ain, United Arab Emirates; <sup>2</sup>Pharmacognosy Department, Faculty of Pharmacy, Egyptian Chinese University, Cairo, Egypt

Correspondence: Mohammad A Khasawneh, United Arab Emirates University, Sheikh Khalifa Bin Zayed St, P.O. Box No. 15551, Asharij, Al-Ain, Abu Dhabi, United Arab Emirates, Tel +971 55 937 6770, Email mohammad.khasawneh@uaeu.ac.ae

**Introduction:** Phyto-nanotechnology offers a sustainable method for synthesizing biocompatible metal nanoparticles (NPs) with therapeutic potential. The diverse medicinal flora in the UAE, particularly *Leptadenia pyrotechnica* (LP), provides a vital resource for advancing this research area. This plant is historically valued in the region for its wide medicinal applications due to its abundance of bioactive compounds.

**Methods:** In this study, eco-friendly, straightforward, and low-temperature hydrothermal synthesis methods were applied to synthesize potentially therapeutic Zn and Fe NPs using LP extracts. The generated NPs were characterized using UV–VIS, FT-IR, SEM, EDX, XRD and DLS. Moreover, they were investigated for their total phenolic and flavonoid contents, along with their antioxidant and skin anticancer effects.

**Results:** The UV–Vis spectra disclosed absorption band at about 275 nm, and the FT-IR confirmed the successful coating of the NPs with the plants' phytochemicals, thus ensuring the successful bio-fabrication of the proposed NPs. SEM/EDX outcomes suggest a more potent reducing effect of the aqueous extract, while a more effective coating of the alcoholic extract. DLS revealed monodispersed NPs, with average sizes ranging from 43.82 to 207.8 nm. LFeC demonstrated the highest phenolic and flavonoid contents (49.96±4.76 µg of GAE/mg of DW and 43.89±2.89 µg of Qu/mg of DW, respectively) and the greatest potency against skin cancer cell lines (IC<sub>50</sub>=263.56 µg/mL). However, LZnC exhibited the strongest radical scavenging effect against DPPH and ABTS radicals (IC<sub>50</sub>=139.45µg/mL and 35.1µg/mL, respectively).

**Discussion:** The results of this study demonstrated that both extracts of LP are effective in the green synthesis of Fe and Zn nanoparticles for biomedical applications, with alcoholic extracts providing superior coating, capping, and stabilizing properties, leading to lower agglomeration, higher carbon content, total phenolic and flavonoid contents, along with enhanced anticancer and antioxidant effects. This work gives a showcase of sustainable materials that are promising for therapeutic applications.

**Keywords:** *Leptadenia pyrotechnica*, skin cancer, antioxidant, green nanoparticles, iron nanoparticles, zinc nanoparticles

## Introduction

Skin cancer has evolved as the most common malignant disease with an average increment of about a million new cases annually.<sup>1</sup> In the UAE skin cancer is reported as one of the top ranked cancers according to Annual Report of the UAE Cancer Incidence.<sup>2,3</sup> Treatment of skin cancers by chemotherapeutic agents often results in the widely unpleasant side effects like myelosuppression, weight loss, alopecia, sterility and neutropenia.<sup>1,4</sup>

Recently, several metals, and their oxide nanoparticles (NPs) were synthesized, and their applications were investigated in various fields of science and technology, including biomedical practices.<sup>5–7</sup> Metal oxide NPs have been synthesized by physical and chemical methods; the chemical methods involve the use of different chemicals as reducing

and stabilizing agents. However, the chemical synthesis strategy has become responsible for various biological and environmental risks due to the toxicity of used chemicals. Hence, recently, biosynthesis of these NPs using plants, algae, and microbes has emerged as a green, simple, inexpensive and energy efficient method as compared to the chemical routes.<sup>8</sup> Utilizing plant extracts in the green synthesis process offers extra merits over extracts of microorganisms. These advantages enclose faster synthesis rate, scalability, and better biocompatibility for human body.<sup>9,10</sup> Generally, biometabolites that are present in plant extracts act as reducing, stabilizing, and capping agents for the metal precursors, causing the production of the desired NPs.<sup>11</sup> The above-mentioned factors make the plant-based NPs excellent candidates for biomedical applications, especially that their tiny sizes allow them to penetrate and travel through the minute blood vessels, capillaries, barriers, and junctions. Hence, improved, and enhanced stability, solubility, bioavailability, and distribution can be achieved in the body, leading to enhanced drug retention in the cells, reduced dosage, and minimal toxicity.<sup>12</sup> Thus, they are promising candidates for drug delivery and development studies. Several research papers described the phytochemical-based NPs to boost plant extract biological activities through enhancing their bioavailability and effectiveness. Thus, plant-based NPs could demonstrate stronger biological activities than the conventional crude extracts of the same plants. Anticancer is one of these pharmacological activities.<sup>13–17</sup>

Among an extensive number of metal NPs, iron and zinc oxide NPs have gained the attention of the scientific community due to their unique properties and potential applications in biomedicine and therapeutics.<sup>18</sup> Plant-mediated iron and zinc oxide NPs demonstrated significant pharmacological activities in numerous research studies, particularly antioxidant, and anticancer activities.<sup>19–22</sup> For instance, zinc oxide NPs that was green-synthesized using aqueous extract of *Limonium pruinosum* demonstrated a good activity against skin cancerous cells when tested in-vitro.<sup>23</sup> Also, iron oxide NPs displayed a distinguishable in-vitro skin anti-cancer effect in several reports.<sup>24,25</sup>

*Leptadenia pyrotechnica* (LP) is a traditional medicinal shrub of the *Asclepiadaceae* family, widely cultivated in the UAE and used in a variety of food preparations. The shrub is commonly used traditionally for treatment of inflammatory diseases and cancer.<sup>26</sup> LP is a source of many pharmacologically active constituents, such as cardenolides, alkaloids, flavonoids, sterols, triterpenes, and polyoxypregnanes.<sup>27</sup> Their anti-tumor effects have been intensively studied.<sup>26–28</sup> In our previous study, 80% ethanolic extract of LP and its fractions (n-hexane, ethyl acetate, n-butanol and aqueous) showed a considerable in-vitro cytotoxicity against colon cancer cell lines.<sup>29</sup>

To date, there is no FDA approved topical treatment for skin cancer. Therefore, the search for innovative anticancer agents with high safety profiles using new technologies is a must nowadays. Furthermore, as discussed above, green NPs can improve penetration of bioactive molecules through human cells like skin and tumors, causing enhanced intracellular and intranuclear bioavailability. Since iron, zinc, and the proposed plant have previously displayed significant antioxidant and anticancer activity, we assume that this combination might lead to the formation of potent skin anticancer natural-based NPs that could be safer than the conventional chemotherapy and with lower side effects. Therefore, the objectives of this study are to investigate the efficiency of UAE wild LP aqueous and alcoholic extracts in the phyto-fabrication of iron, and zinc NPs and their possible application as antioxidant and skin anticancer agents. It is worth mentioning that this is the first study on the bio-fabrication, physicochemical and biological investigations of Fe and Zn NPs using LP extracts.

## Material and Methods

### Chemicals

Ethanol (puriss., absolute, 99.8%), methanol (gradient grade for liquid chromatography LiChrosolv<sup>®</sup> Reag., 99.9%) was purchased from Honeywell, Germany.

Iron (III) chloride hexahydrate (ACS reagent, 97%), zinc acetate-2-hydrate extra pure, potassium bromide (anhydrous, free-flow), folin and ciocalteu's phenol reagent, gallic acid-1-hydrate extra pure, aluminum chloride 98%, potassium acetate reagent plus  $\geq 99.0\%$ , sodium carbonate, and quercetin, 2,2-diphenyl-1-picrylhydrazyl (DPPH), potassium persulfate (99+%, ACS reagent), 6-hydroxy-2,5,7,8-tetramethylchroman-2-carboxylic acid (Trolox), 2,2'-azino-bis(3-ethylbenzothiazoline-6-sulfonic acid (ABTS) were purchased from Sigma Aldrich, Germany.

## Preparation of LP Extracts

Fresh samples of the aerial parts of *L. pyrotechnica* (Forssk). Decne. (stem, fruit) were harvested in June 2022 from the farms of the United Arab Emirates University in Al-Ain, UAE. Dr. Mohamed Taher, the head of the herbarium in the Biology department at the university, authenticated the plant materials. A voucher specimen, labeled with the serial number UAEU-NH0014686, was archived in the herbarium of the College of Science at the United Arab Emirates University. Subsequently, the freshly collected materials underwent drying and crushing using a household blender. The resulting dried powders were then employed in the preparation of aqueous and hydro-alcoholic extracts through decoction and maceration, respectively. Decoction entailed heating 265.76 g of the plant materials in 1.5 L deionized water at 60°C for 3 hours with continuous stirring at 1500 RPM. Conversely, the hydro-alcoholic extract was prepared by macerating 265.76 g of the plant's crushed powder in 80% ethanol (1.5 L) for three days. Following this, filtration and evaporation processes were executed to obtain the aqueous and alcoholic crude extracts. Evaporation was carried out to achieve dry crude extract at 60°C and 72–175 mbar, using Buchi Rotavapor R-200 equipped with Buchi heating bath B-490, Buchi vacuum pump interface I-300, V600, and Julabo cooling system FP50 (Germany). Exhaustive extraction was performed for both types of extracts by repeating the preceding steps multiple times to ensure complete extraction of the phytochemicals from the extracts. The total amount obtained for each crude extract was 54.01 gm for the hydro-alcoholic extract and 69.24 gm for the aqueous extract, with concentrations of 203 mg/gm dry weight and 260.5 mg/gm dry weight, respectively. The % yields of the final crude extracts were 20.3226% and 26.053%, respectively, which were calculated by dividing the weight of the produced crude dry extract by the weight of the dry plant powder used for the extraction process.<sup>30</sup>

## Synthesis of the Nanoparticles

The green Fe NPs were bio-fabricated using both aqueous and 80% ethanolic extracts, following a previously published method with some modifications.<sup>31</sup> In summary, 100 mL of the extract (20 mg/mL) was added to 300 mL of 0.02M FeCl<sub>3</sub>•6H<sub>2</sub>O, dissolved in 300 mL deionized water. The immediate color change from yellow to black indicated the formation of Fe NPs. Subsequently, the mixture was refluxed for 90 minutes at 55–60°C with stirring at 500 RPM using a Witeg MSH-20D hotplate from Germany, facilitating nucleation and growth of the NPs. For the biosynthesis of ZnO NPs, the process followed Ashraf et al method with some adjustments.<sup>32</sup> Initially, 10 mL of zinc acetate dihydrate (10 g) was mixed with 100 mL of plant extract (2.61 gm and 2.03 gm for aqueous and alcoholic extracts, respectively) and stirred for 3 hours at 55–60°C and 500 RPM. After completion, the mixture was allowed to cool, and precipitates were obtained via centrifugation. The pellets were washed and centrifuged three times with distilled water, then ethanol at 4000 RPM for 3–5 minutes. The resulting NPs underwent air drying, were weighed, and stored for further analysis. To ensure purity, the formed NPs were washed three times with deionized water and ethanol, followed by centrifugation at 4000 RPM for 3–5 minutes using the Ohaus FC5714 Frontier 5000 Series Multi Pro Centrifuge. The resulting supernatants were air-dried to prevent decomposition of bioactive constituents from the extracts. These bioactive metabolites accelerate the reduction of metal precursors, contribute to NPs' coating, and enhance the stability and biological activity of the NPs. Reactions were performed at temperatures below 60°C for the same reason.<sup>33</sup> After complete dryness, the NPs were ground and stored for subsequent characterization and biological investigations. It is worth mentioning that the purpose of using two types of extracts is that we need to monitor the effect of extraction method on the physiochemical and biological quality of the synthesized green NPs to obtain the highest quality and the most potent NPs, especially that different extraction solvents extract different types of active constituents.<sup>34</sup>

## Characterization of the Nanoparticles

The bio-fabricated NPs underwent characterization through various techniques, including Dynamic Light Scattering (DLS), UV–Vis Spectrophotometry, Scanning Electron Microscope equipped with Energy-Dispersive X-Ray Spectroscopy (SEM/EDX), X-ray diffraction (XRD), and Fourier-transform infrared Spectrophotometry (FT-IR) analysis. DLS provides insights into the size range, agglomeration state, and surface charge of the NPs. Additionally, SEM play crucial roles in determining size, shape, surface morphology, and agglomeration state, as well as visualizing the

capping of NPs with organic compounds from the extracts. EDAX was utilized for elemental composition analysis of the metal NPs. In contrast, FT-IR contributes to the molecular analysis of the organic compounds that are coating the NPs. XRD and UV-Vis Spectrophotometry were employed to evaluate the crystallinity and optical properties of the resulting NPs, respectively.<sup>35,36</sup>

### Powder X-Ray Diffraction (PXRD)

The XRD patterns of the under-investigation NPs generated through biological processes were captured using a Rigaku MiniFlex 600-C Benchtop Powder X-Ray Diffraction (XRD) Instrument from Rigaku Co. Instruments, USA. CuK $\alpha$  X-ray ( $\lambda = 1.542 \text{ \AA}$ ) was utilized at 40 kV and 15 mA. A continuous scan at  $2\theta/\theta$  angles spanning from  $10^\circ$  to  $80^\circ$  was applied for samples' analyses, with a scanning rate of  $1^\circ/\text{min}$ . The matching and analysis of the resulting peaks were conducted via Match software.

### Scanning electron microscope (SEM) and energy-dispersive X-ray spectroscopy (EDX)

Images of the final NPs were captured, and their elemental compositions were mapped utilizing the Quattro scanning electron microscope with an EDX detector from Thermo Fisher Scientific, USA. The instrument was run under high vacuum conditions and accelerated voltage ranging from 10 to 30 kV, with a magnification set within the range of 10,000 and 20,000 X.

### Dynamic Light Scattering (DLS)

Mean particle size and zeta potential of NPs were assessed using Malvern Zetasizer Nano, utilizing Dynamic Light Scattering (DLS). Before conducting measurements, the samples were diluted with ethanol to attain an optimal scattering intensity. The measurements were carried out at  $25^\circ\text{C}$  with a flow rate of 0.500, using a measurement position of 2 mm and 4.65 mm for zeta and size analyses, respectively. Zeta potentials and particle sizes for the investigated samples were determined by calculating the average of three runs.

### UV Visible Spectrophotometer

The Plasmon resonance of the newly formed NPs was identified through measurements of the suspended NPs in 50% ethyl alcohol via Cary 60 UV-Vis Spectrophotometer from Agilent Technologies Ltd, Malaysia. Spectral data within the 200–800 nm range were recorded to pinpoint the characteristic peaks validating the fabrication of Fe and Zn NPs.

### Fourier-Transform Infrared (FT-IR) Spectroscopy

FT-IR spectrum of NPs was recorded using Nicolet NEXUS 470 Fourier-transform infrared Spectrophotometer from Thermo Scientific, USA and was employed to analyze the functional groups of the organic phytochemical constituents involved in capping of the NPs, along with determining peaks related to the metal itself. The samples, weighing 0.002 g, were thoroughly ground and added to 0.2 g KBr. The resulting mixture was compressed using a hydrolytic compressor to make a thin disc, which was subjected to analysis spanning the range of  $400\text{--}4000 \text{ cm}^{-1}$ . The analysis parameters were set at an average of 64 scans at a  $25 \text{ cm}^{-1}$  spectral resolution and a laser frequency of  $15798.3 \text{ cm}^{-1}$ . The spectrum was detected in transmittance % mode.

## Chemical Investigation of the Total Phenolic and Flavonoid Contents

### Total Phenolic Content (TPC)

The total phenolic contents of the LP-mediated fabricated NPs were determined by performing the Folin-Ciocalteu assay.<sup>37</sup> This method relies on the capacity of phenolic compounds to reduce Folin-Ciocalteu reagent, resulting in the formation of molybdenum-tungsten complexes exhibiting a blue color, which can be quantified spectrophotometrically. The color intensity correlates linearly with the concentration of phenolic compounds in the reaction medium.<sup>38</sup> In brief, 100  $\mu\text{L}$  of 1 mg/mL of the sample was mixed with 125  $\mu\text{L}$  of Folin-Ciocalteu reagent and 750  $\mu\text{L}$  of sodium carbonate solution (15% w/v) in a test tube. The final volume was completed to 5 mL with distilled water and thoroughly mixed. A blank was prepared in a similar manner, replacing the sample with the solvent, 80% methanol, used for sample solubilization. The mixture was then incubated for 90 minutes in the dark at room temperature, then measured at 765 nm using a Cary 60 UV-Vis Spectrophotometer (Agilent Technologies Ltd, Malaysia). The total phenolic content (TPC) of

the sample was calculated as micrograms of gallic acid equivalents per milligram of dry weight of the sample ( $\mu\text{g}$  of GAE/mg of DW), using the samples' average absorbances and the linear equation ( $y = 0.0023x - 0.047$ ) of the standard curve plotted with gallic acid. To prepare this standard curve, gallic acid was dissolved in 80% methanol at a concentration of 1 mg/mL as a stock solution, which was then further diluted to different concentrations (40, 80, 120, 160, 200, 240, and 280  $\mu\text{g}/\text{mL}$ ). The prepared concentrations were subjected to the same procedures as the samples, with blanks prepared similarly by replacing the sample with the solvent. The resulting average absorbances were constructed against their respective concentrations. All measurements were conducted in triplicate and presented as mean  $\pm$  standard deviation (SD).

### Total Flavonoid Content (TFC)

The total flavonoid contents within the LP corresponding green-synthesized NPs were examined using the Aluminum chloride colorimetric assay.<sup>37</sup> This method relies on the interaction between flavonoids and aluminum chloride, leading to the formation of colored, stable flavonoid-aluminum complexes involving the C-4 keto group and either the C-3 or C-5 hydroxyl group of flavones and flavonols, which are subsequently quantified spectrophotometrically.<sup>39</sup> In summary, the samples were prepared by mixing them with an appropriate solvent (80% methanol) to attain a concentration of 1 mg/mL. Then, in a test tube, 0.5 mL of the sample was mixed with 0.1 mL of 10%  $\text{AlCl}_3$ , 0.1 mL of 1 M potassium acetate, and 1.5 mL of 95% methanol. The volume was filled to 5 mL with distilled water and mixed. A blank was prepared following the same procedure, substituting the sample with 80% methanol. Finally, the mixture was incubated for 60 minutes at room temperature in darkness, after which the absorbance was measured at 415 nm using a Cary 60 UV-Vis Spectrophotometer, Agilent Technologies Ltd, Malaysia. The total flavonoid content was expressed as  $\mu\text{g}$  of quercetin equivalents per milligram dry weight of the sample ( $\mu\text{g}$  Qu/mg of DW), and it was calculated using the linear equation derived from the standard curve of quercetin ( $y = 0.0066x + 0.0143$ ). The preparation of the quercetin standard curve involved the preparation of various concentrations of quercetin, ranging from 5 to 100  $\mu\text{g}/\text{mL}$ , from a stock solution at a concentration of 1 mg/mL. These prepared concentrations underwent the same procedure as described above instead of the sample, and the resulting average absorbances were plotted against their concentrations. All measurements were carried out in triplicates and presented as mean values with accompanying standard deviations (SD).

### In-Vitro Evaluation of the Antioxidant Activity

The antioxidant properties of the LP NPs were assessed using DPPH and ABTS colorimetric radical scavenging assays, following established protocols with slight adjustments.<sup>40-44</sup> For the DPPH assay, samples were dissolved in 80% methanol to prepare stock solutions. These solutions were then diluted to six concentrations (10, 20, 40, 60, 80, 100  $\mu\text{g}/\text{mL}$ ) and mixed with 0.2 mM DPPH with a ratio of 2:1 v/v before incubating in darkness at room temperature for 40 minutes. Methanol 80% mixed with the DPPH served as the negative control, and a sample blank comprising the dispersed sample in 80% methanol was employed for each concentration of the NPs under examination due to their dispersion in the solvent and low solubility which affects the absorbance readings and might give false results. Subsequently, the absorbance was determined at 517 nm using a UV microplate reader (Hidex Sense, Hidex, Turku, Finland).

- The % radical scavenging activity of the samples under investigation was estimated using the following formula:

$$\left[ \left( \frac{A_b - A}{A_b} \right) \times 100 \right]$$

Where  $A_b$  is the absorbance of the negative control and  $A$  is the absorbance of the sample. The determination of  $\text{IC}_{50}$  ( $\mu\text{g}/\text{mL}$ ) values involved constructing a calibration curve within the linear range for each sample under investigation. This process entailed plotting the concentration of the sample against its corresponding percentage of radical scavenging. The  $\text{IC}_{50}$  represents the concentration at which the samples reduce DPPH absorption by 50%; hence, a lower  $\text{IC}_{50}$  indicates higher antioxidant activity. In the ABTS radical scavenging assay, stock solutions of the samples and positive control (TROLOX) were prepared at a concentration of 100  $\mu\text{g}/\text{mL}$  in 80% methanol. Subsequently, various

concentrations (10, 20, 40, 60, 80, and 100 µg/mL) were derived from these stock solutions for testing purposes. The formation of the ABTS+• radical cation involved mixing 7 mM of ABTS with 2.45 mM potassium persulfate in a 1:1 ratio, followed by incubation in darkness for 12–16 hours. The resulting mixture was then diluted with methyl alcohol until an absorbance value of 0.70±0.02 at 734 nm was attained. Following this, 100 µL of each sample concentration solution was mixed with 100 µL of the diluted ABTS+• and incubated for 10 minutes in darkness at room temperature in a 96-well plate. Finally, the absorbance of the plate was measured at 734 nm using a UV microplate reader (Hidex Sense, Hidex, Turku, Finland). Methanol 80% with ABTS+• served as the negative control, while a sample blank consisting of the sample dispersed in 80% methanol was employed for each concentration of the tested NPs due to their poor solubility and uniform dispersion in the solvent.

- The percentage radical scavenging effect was estimated using the following formula:

$$\left[ \left( \frac{A_c - A}{A_c} \right) \times 100 \right]$$

Where  $A_c$  is the absorbance of the -ve control, and  $A$  is the absorbance of the sample. Using a calibration curve within the linear range, the  $IC_{50}$  (µg/mL) values were determined by correlating extract concentrations with their corresponding percentages of radical scavenging. Similar to DPPH assays, a higher  $IC_{50}$  value indicates lower antioxidant activity, as it signifies the concentration needed by the sample to reduce ABTS absorption by 50%. All measurements were conducted in triplicate and presented as mean ± standard error (SE).

## Investigation of Skin Anticancer Activity (in-vitro)

### Cell Culture

Cultured cell lines originating from A-431 human epidermoid skin carcinoma (skin/epidermis) were procured from Nawah Scientific Inc., situated in Mokattam, Cairo, Egypt. These cell lines were nurtured in DMEM media, complemented with 100 mg/mL of streptomycin, 100 units/mL of penicillin, and 10% heat-inactivated fetal bovine serum. The ongoing maintenance of these cell lines was conducted within a humidified environment with 5% (v/v)  $CO_2$  at 37 °C.

### Cytotoxicity Assay

Cell viability was assessed using the Sulforhodamine B (SRB) assay. In 96-well plates, 100 µL of cell suspension ( $5 \times 10^3$  cells per well) was dispensed and allowed to incubate in complete media for 24 hours. Following this, the cells were subjected to various concentrations (0.1, 1, 10, 100, 1000 µg/mL) of the bio-formed NPs by treating them with another 100 µL of media containing the NPs. After 72 hours of the NPs exposure, the cells were fixed by replacing the media with 150 µL of 10% trichloroacetic acid (TCA) and incubating at 4 °C for 1 hour. Post-TCA removal, the cells were washed five times with distilled water. Subsequently, 70 µL of SRB solution (0.4% w/v) was added to the plates and incubated in darkness at room temperature for 10 minutes. The plates were then washed three times with 1% acetic acid and left to air-dry overnight. Finally, 150 µL of TRIS (10 mM) was added to dissolve the protein-bound SRB stain, and the absorbance was measured at 540 nm using a BMG LABTECH®- FLUOstar Omega microplate reader (Ortenberg, Germany). Negative control wells that did not include drugs were assessed as well.<sup>45,46</sup>

## Results and Discussion

### Characterization of the Nanoparticles

Figure 1 shows the resulted LP-based NPs. LZnC and LFeC are the zinc and iron NPs which were synthesized using the alcoholic extract, respectively, while LZnQ and LFeQ are the zinc and iron NPs which were fabricated utilizing the aqueous extract, respectively.

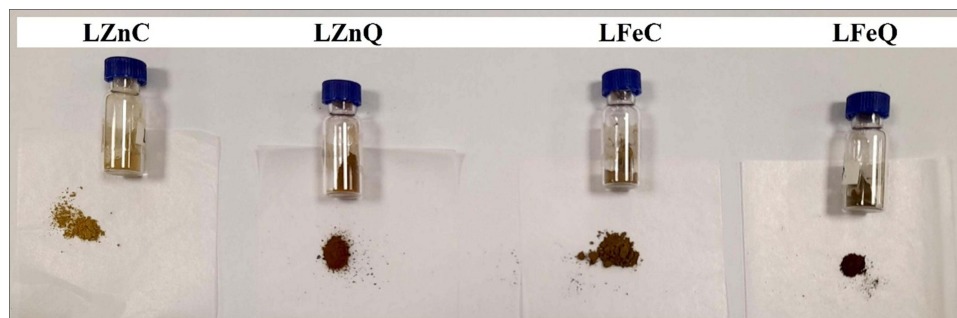


**Figure 1** The resulted phyto NPs using LP alcoholic and aqueous extracts.

### Powder X-Ray Diffraction (PXRD)

A Bragg's angle X-ray powder diffractometer, covering angles from  $10^\circ$  to  $80^\circ$ , was utilized to ascertain the crystalline structure, nature, and phase composition of the synthesized NPs. As shown in **Figure 2A**, the XRD patterns acquired for the NPs synthesized using LP extracts indicate an amorphous structure with a limited crystalline nature.

### Scanning Electron Microscope (SEM) and Energy-Dispersive X-Ray Spectroscopy (EDX)

Morphology of the surface and agglomeration state of the bio-fabricated NPs were observed using SEM. The resulted images revealed a fluffy to medium rough and irregular-like surface appearance, showing a higher tendency for agglomeration in the

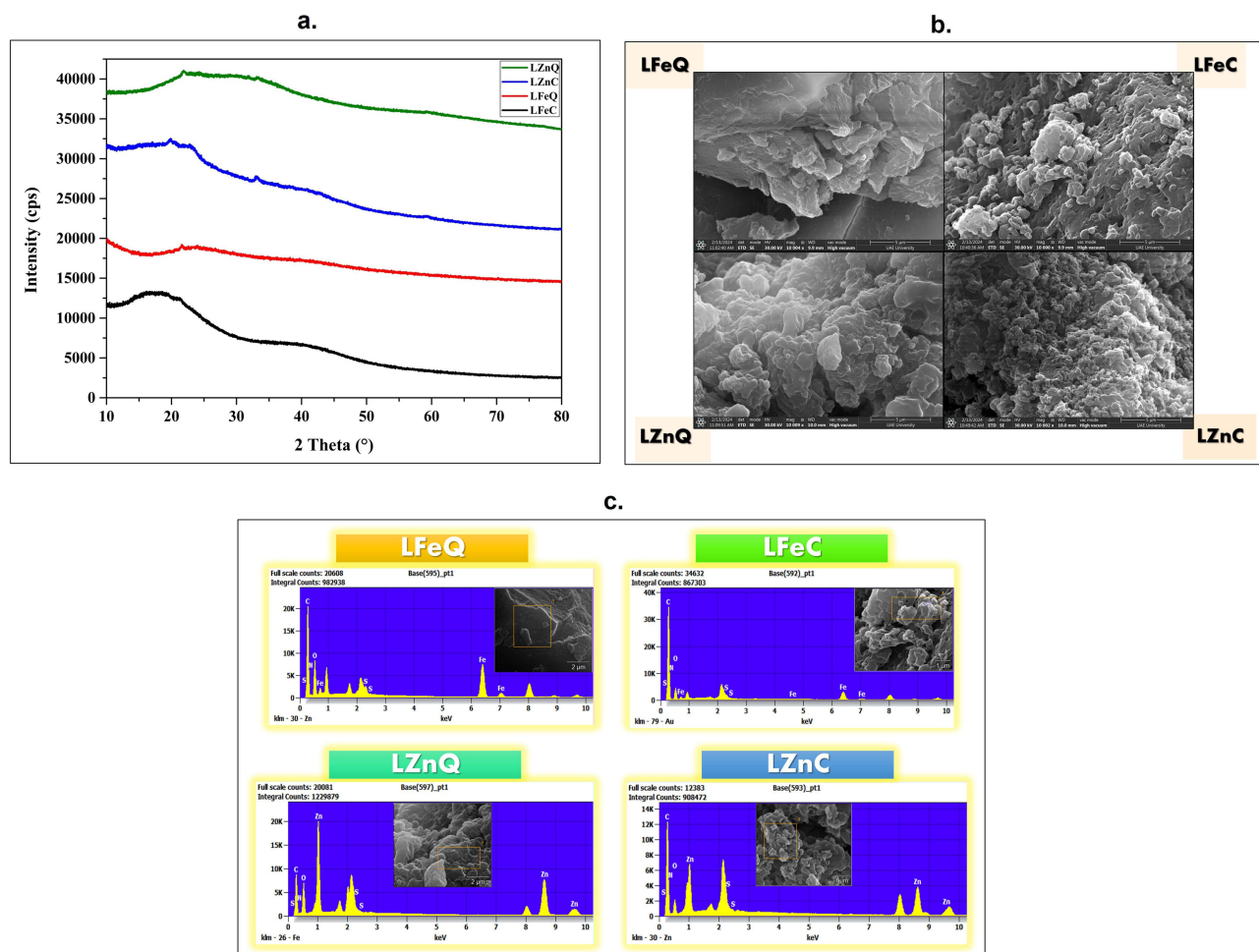


**Figure 2** (a) XRD patterns, (b) SEM images, (c) EDX analysis of the bio-fabricated LP-mediated Fe and Zn NPs.

case of LFeQ and LZnQ compared to NPs prepared via the plant's alcoholic extract as shown in Figure 2B. This suggests that *L. pyrotechnica* alcoholic extract may offer better coating for its corresponding NPs than aqueous extracts. In general, several previous studies have consistently reported that green-synthesized NPs tend to agglomerate due to the adhesive nature of the plant extracts utilized.<sup>31,47–52</sup> Among the formed NPs, LZnC NPs demonstrated the most uniformity, dispersion, and homogeneity. EDX analysis was utilized to validate the formation of Fe and Zn NPs and to explore the elemental composition of their phytochemical coating. The presence of discernible peaks corresponding to iron and zinc unequivocally confirms the successful synthesis of Fe and Zn NPs. Examination of the samples revealed that the mean weight percentages (wt.%) of iron were 8.17% and 16.74% for LFeC and LFeQ NPs, respectively, and 25.54% and 39.86% for LZnC and LZnQ NPs, respectively. Furthermore, oxygen and carbon peaks were identified within the 0.1 to 0.5 KeV range, exhibiting oxygen proportions of 28.87%, 36.13%, 19.03%, and 27.47%, and carbon percentages of 43.49%, 27.63%, 47.85%, and 29.16% in LFeC, LFeQ, LZnC, and LZnQ NPs, respectively. Also, nitrogen was detected with weights ranging from 3.51% to 19.5% in the tested samples, indicating the presence of nitrogenous phytochemicals among the coating that presents around the green NPs. Moreover, the presence of additional elements such as sulfur is attributed to the phytochemicals from the plant acting as capping and coating agents for the NPs (Figures 2C and 3). It can be concluded from these findings that the concentrations of Fe and Zn are higher in the aqueous-based NPs compared to their alcoholic counterparts, suggesting a more potent reducing effect of the aqueous extract. Conversely, the proportion of the carbon element is higher in the alcoholic-based NPs, hinting at a more effective coating provided by the phytochemicals from the alcoholic extract. This observation is consistent with the SEM images that showed a decreased tendency of agglomeration in the NPs derived from alcoholic extract. It implies that this outcome is due to their higher coating and capping with phytochemicals, resulting in enhanced stability and dispersion for the NPs derived from alcoholic extract compared to those derived from aqueous extract.

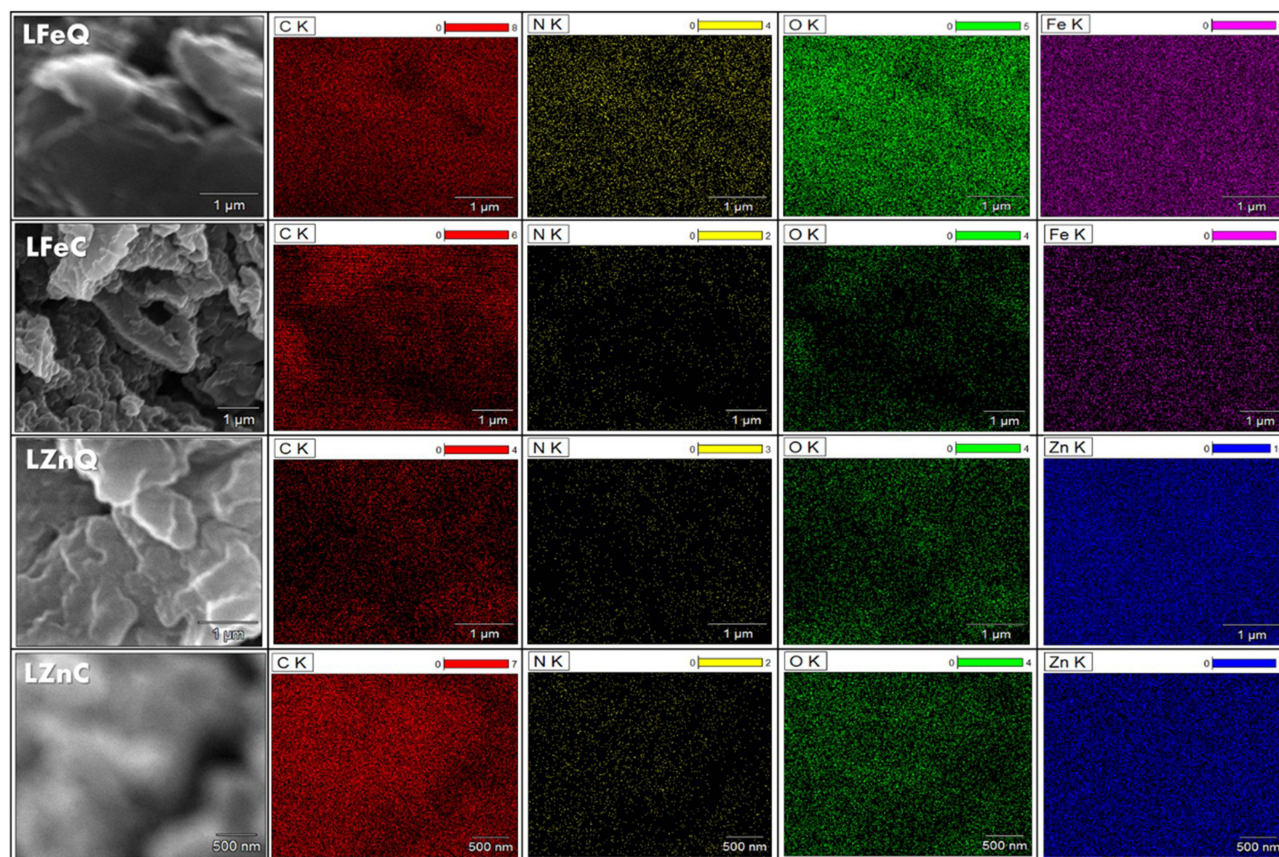


**Figure 3** EDS mapping of Fe, Zn, C, N, O elements in the bio-fabricated LP-mediated Zn and Fe NPs.



## Dynamic Light Scattering (DLS)

Malvern Zetasizer DLS was employed to assess the particle size, zeta potential values, and polydispersity indices of the biosynthesized NPs dispersed in ethanol at ambient temperature. Zeta potential gives an idea about the NPs' stability by measuring the repulsion between neighboring particles carrying similar charges, and so correlating with the stability of colloidal dispersions. A higher zeta potential value signifies enhanced particle stability. Additionally, the polydispersity index is crucial for evaluating homogeneity of the particle size in the tested sample, where elevated values reflect greater heterogeneity among particles.<sup>53</sup> The resulting data is displayed in Table 1, and particle size along with zeta potential distribution graphs for all the investigated samples are illustrated in the Figure 4. According to the provided values, LZnC displayed the smallest particle size (43.82 nm), showcasing the superior monodispersity with polydispersity index value of 0, followed by LFeQ, then LZnQ and LFeC. Conversely, the highest stability was displayed in LFeQ, which exhibited a positive zeta-potential value of 24.8, followed by LFeC, then LZnC and LZnQ. Thus, it is explicit from the tabulated values of PDI and zeta potential that all of the samples are showing monodispersity, and positive surface charge. Moreover, LP-based Fe NPs are showing higher stability than Zn NPs.

## UV Visible Spectrophotometer

The UV–visible absorption spectra of LP-coated Fe and Zn NPs are illustrated in Figure 5A, confirming the occurrence of surface plasmon resonance. The distinctive absorption peaks at 275 nm in LFeC and LFeQ NP samples, indicate the formation of Fe NPs. Additionally, the confirmation of Zn presence in HZnC and HZnQ samples is evident through optical transitions observed at 275 nm. Typically, iron and zinc NPs exhibit a broad peak in the UV–visible spectrum within the ranges of 220–288 nm and 230–330 nm, respectively.<sup>31,54,55</sup>

## Fourier-Transform Infrared (FT-IR) Spectroscopy

FT-IR analysis serves as a reliable approach to scrutinize the molecular composition of the examined extracts and the surface functionalization of their corresponding Fe and Zn NPs. The resulting spectra, presented in the Figure 5b offer valuable insights. Within the 3214–3542  $\text{cm}^{-1}$  range, the broad bands suggest O–H stretching associated with carboxyl acid (usually carboxylic acids are widely ranged 2500–3500  $\text{cm}^{-1}$ ) and alcoholic hydroxyl groups, while the narrow peaks in the 2780–2928  $\text{cm}^{-1}$  range signify aliphatic C–H stretching. Vibrations between 2101–2398  $\text{cm}^{-1}$  indicate C≡N and C≡C, and strong bands around 1622–1922  $\text{cm}^{-1}$  confirm the presence of C=O and C=C functional groups. Nitro compounds are represented by bands between 1325.53–1511.02  $\text{cm}^{-1}$ , and C–O vibrations are authenticated in the spectra at 1033.67–1271.86  $\text{cm}^{-1}$ . Bands of aromatic rings, halogenic compounds, and organometallics (Zn-O and Fe-O) are shown at lower frequencies from 487.93 to 893.81  $\text{cm}^{-1}$ .<sup>56</sup> The resulted FT-IR spectra prove the existence of various functional groups, including carbonyls, alcoholic, phenolic, alkenes, alkanes, alkynes, nitro, alkyl halides, and aromatic, pointing to the existence of diverse phytochemical classes such as phenolics, fatty acids, flavonoids, saponins, amino acids, quinones, and terpenoids. This confirms the effective encapsulation of the generated green NPs with the LP chemical components. Comparing FT-IR spectra, a close resemblance is observed between LP extracts and their respective NPs, confirming the environmentally friendly synthesis and coating of the LP-based iron and zinc NPs as proposed in this study. The variation in the intensity of certain bands or their absence in the analyzed NPs compared to their corresponding extracts is postulated to result from the depletion or

**Table 1** Mean Particle Size, Zeta Potential Values and Polydispersity Indices of the Synthesized Green NPs According to NNLS Fitting

NP	Size (d.nm)	Zeta Potential (mV)	PDI
LFeC	163, 207.8	22.2	0.01, 0.005
LFeQ	94.77, 59.6	24.8	0.01, 0.002
LZnC	43.82	17.9	0
LZnQ	160.5	17.8	0.015

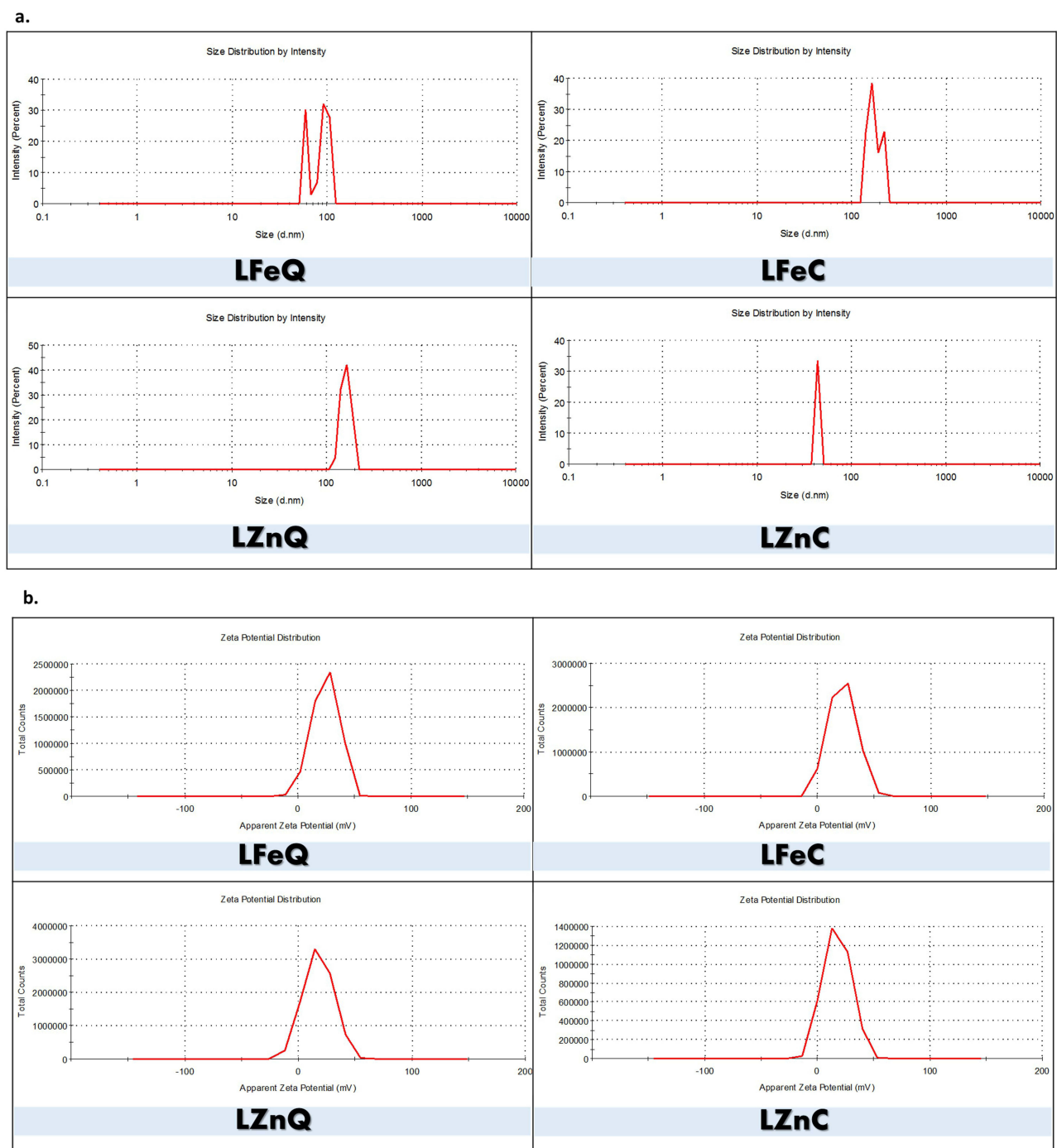


**Figure 4** (a) Size and (b) Zeta potential distributions of the bio-synthesized Zn and Fe NPs using both aqueous and 80% ethanolic extracts.

excessive production of these functional groups following the reduction reaction involving the phytochemical constituents of LP extracts and the metal precursor. These results are in agreement with previous reports.<sup>23,31,54,57,58</sup>

## Chemical Investigation of Total Phenolic and Flavonoid Contents (TPC and TFC) Total Phenolic and Flavonoid Contents

Phenolic and flavonoid compounds are recognized as principal secondary metabolites present across a wide array of plant species. These compounds play pivotal roles in the synthesis of NPs by the reduction of metal ions. Demonstrating robust

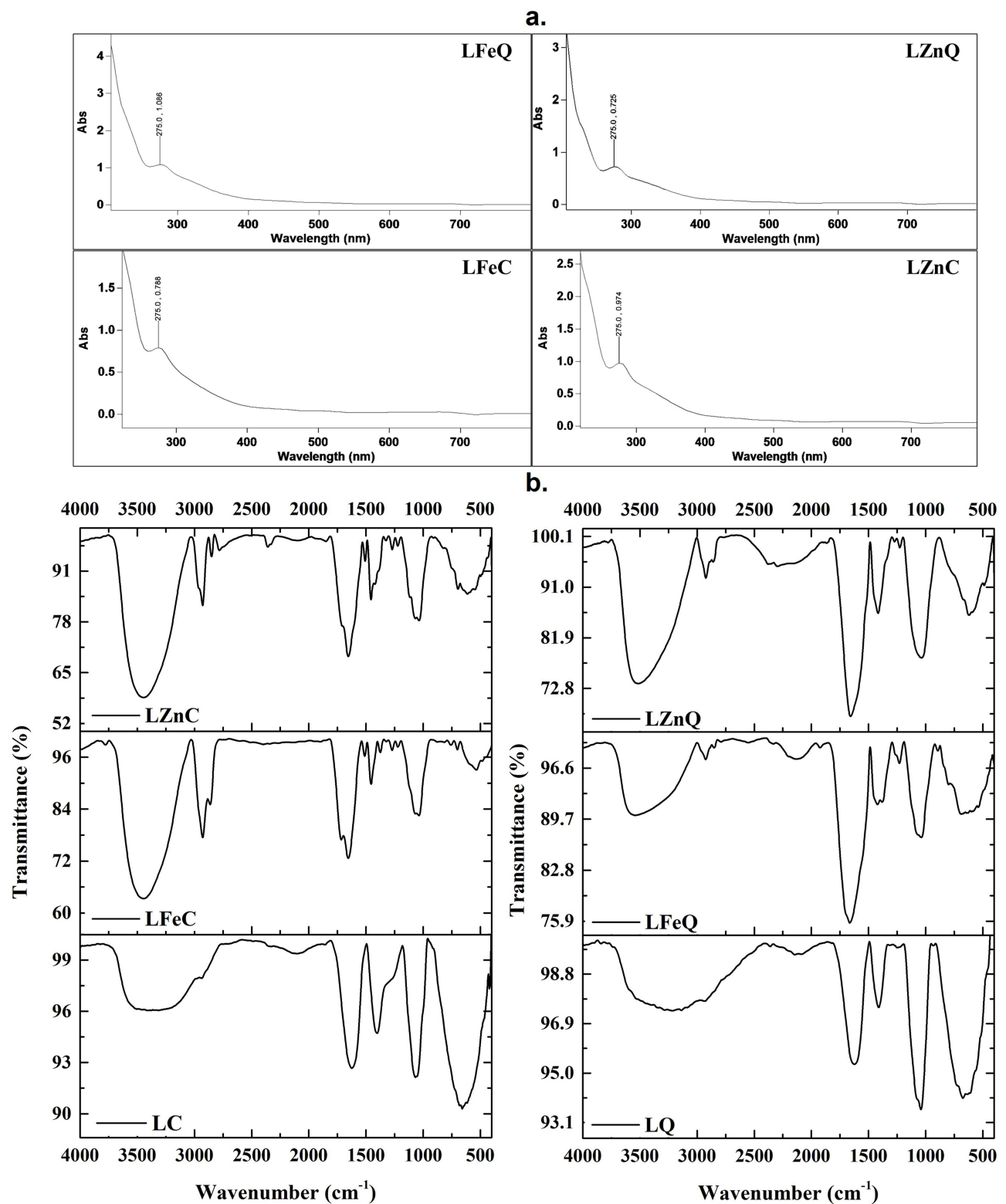


**Figure 5** (a) UV-Vis spectra of LP-based Zn and Fe NPs, (b) FT-IR spectra of ethanolic and aqueous extracts of LP, in addition to their corresponding Zn and Fe NPs.

**Table 2** Total Phenolic and Flavonoid Contents of the Bio-Formulated Green NPs. Results are Presented as Means  $\pm$  SD (n = 3)

	LZnC	LFeC	LZnQ	LFeQ
TPC ( $\mu\text{g}$ of GAE/l mg of DW)	43.29 $\pm$ 3.84	49.96 $\pm$ 4.76	39.57 $\pm$ 5.62	39.91 $\pm$ 1.91
TFC ( $\mu\text{g}$ of QU/l mg of DW)	43.89 $\pm$ 2.89	43.14 $\pm$ 0.67	7.90 $\pm$ 0.64	6.54 $\pm$ 1.23

reducing capabilities, efficient capping, and stabilizing properties, these metabolites exert strong control over the kinetics of nucleation and growth, thereby ensuring the production of metal NPs tailored for specific applications.<sup>59–61</sup> Additionally, their (phenolics' and flavonoids') well-documented efficacy in combating various diseases, including their antioxidant and anticancer potentials attributed to their redox properties, further emphasize their significance.<sup>62</sup> Consequently, the potent reducing ability, antioxidant, and anticancer effects of plants are usually associated with their phenolic and flavonoid contents. Thus, we conducted an investigation into the phenolic and flavonoid contents of the plant-based green NPs. The results of the investigation revealed that all the tested samples contain considerable amounts of both tested classes (Table 2). Furthermore, it is worth noting that the alcoholic-based Fe and Zn NPs contain higher phenolic and flavonoid content compared to their aqueous-based counterparts, giving that LFeC and LZnC demonstrate the highest phenolic and flavonoid contents among the tested samples, respectively ( $49.96 \pm 4.76 \mu\text{g}$  of GAE/mg of DW and  $43.89 \pm 2.89 \mu\text{g}$  of Qu/mg of DW, respectively).

## Evaluation of Antioxidant Activity (in-vitro)

The radical scavenging capabilities or antioxidative properties of natural products derived NPs against ABTS and DPPH radicals are frequently investigated by employing the in-vitro ABTS and DPPH radical scavenging assays. In general, free radicals pose foreign and deleterious threats to our biological milieu. These applied assays are both spectrophotometric in nature, relying on the attenuation of the stable colored ABTS $\cdot+$  and DPPH $\cdot+$  radicals.<sup>63</sup> The fundamental premise of the ABTS assay lies in the generation of a bluish-green radical ABTS $\cdot+$  that is subsequently reduced by antioxidant agents to form colorless ABTS; conversely, the DPPH assay entails the reduction of the purple DPPH $\cdot+$  radical to colorless DPPH.<sup>64</sup> Notably, the principal divergence between these assay methodologies is that ABTS radicals demonstrate a propensity for reaction via the Sequential Proton Loss Electron Transfer (SPLET) mechanism in aqueous solutions, whereas DPPH radicals undergo SPLET-mediated reactions in solvents such as ethanol and methanol.<sup>65–67</sup> Consequently, we have employed both assays to elucidate the antioxidative potential of the bio-fabricated LP-based NPs. The resultant data is quantified as radical scavenging % (Figure 6) wherein a higher value denotes heightened antioxidant efficacy. Additionally, these results are depicted as IC<sub>50</sub> values (Table 3), denoting the concentration at which 50% scavenging of radicals is induced by the tested sample. Lower IC<sub>50</sub> values are indicative of superior antioxidant potency in the examined sample. Our findings reveal significant antioxidant activity across all the tested samples, attributable to the dose-dependent scavenging of DPPH and ABTS free radicals.<sup>23,68,69</sup> Notably, in both DPPH and ABTS assays, LZnC

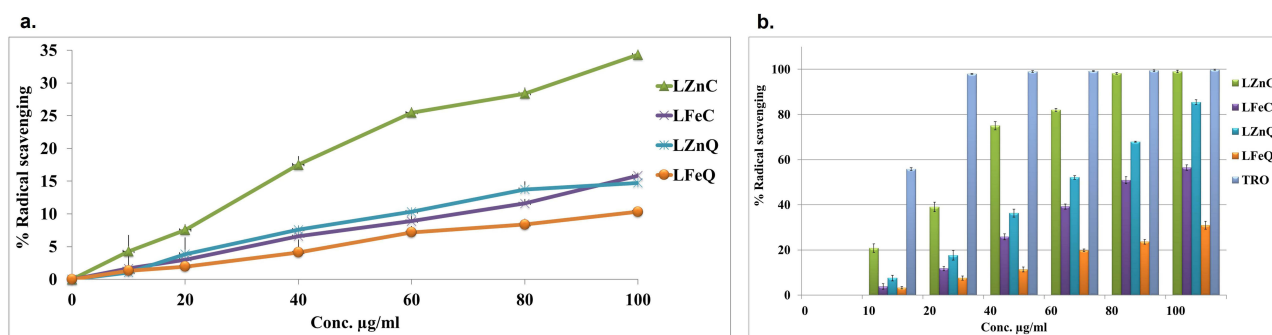


**Figure 6** In vitro antioxidant potential: (a) DPPH and (b) ABTS activities of the samples under study. Data are presented as means  $\pm$  SE (n = 3).

**Table 3** IC<sub>50</sub> Values of the Samples Under Study via DPPH and ABTS Assays

	IC <sub>50</sub> (µg/mL)			
	LZnC	LFcC	LZnQ	LFcQ
DPPH	139.45	327.02	316.77	476.51
ABTS	35.1	82.65	58.16	163.85

demonstrated the most pronounced antioxidant effect across all the tested concentrations, exhibiting an IC<sub>50</sub> of 139.45 µg/mL and 35.1 µg/mL, respectively, showing a radical scavenging percentile of 34.33% and 99% at 100 µg/mL, respectively. This is followed by LZnQ (IC<sub>50</sub> = 316.77 µg/mL and 58.16 µg/mL). Consequently, our findings suggest that LP-based Zn NPs (LZnC and LZnQ) manifest greater radical scavenging efficacy against DPPH and ABTS radicals compared to their Fe counterparts, with LZnC emerging as the most potent candidate against both tested radicals. In a previous study, the authors succeeded to biosynthesis LP-based bimetallic Ag/ZnO NPs which demonstrated a radical scavenging percentage of 99% at 100 µg/mL against DPPH radicals.<sup>68</sup> We can observe a relationship between the phenolic and flavonoid contents of the tested samples and their generated antioxidant effects since it is lucid that the alcoholic extract-based NPs are higher than their aqueous-based analogues in TPC, TFC, ABTS and DPPH radical scavenging capacities. This means that the phenolic and flavonoid contents of the plant extracts involved in the NPs' synthesis acted as a coating and capping agent for the NPs, providing them with stronger antioxidant capability against several types of radicals, especially that phenolics and flavonoids are known as potent antioxidant candidates.<sup>62</sup> These findings have been proven in several previous reports.<sup>70,71</sup> For instance, Somayeh et al successfully synthesized *Satureja intermedia*-mediated silver NPs which exhibited high phenolic, flavonoid contents and thus antioxidant effect.<sup>69</sup>

### Investigation of Skin Anticancer Activity (in-vitro)

The anticancer potential of LP phyto-fabricated NPs was investigated against A-431 human epidermoid skin carcinoma through conducting the sulforhodamine B (SRB) screening assay. The SRB assay stands as a prevalent technique for assessing cytotoxicity in cell-based investigations by quantifying cell density through the measurement of cellular protein content. This method relies on the affinity of SRB, which is a xanthene dye, for basic amino acid residues (proteins) under slightly acidic conditions, which can be subsequently disconnected under basic treatment conditions. Thus, the quantification of bound SRB to cells through colorimetric analysis serves as a proxy for cell density and, consequently, cell proliferation.<sup>45</sup> The outcomes are presented as the percentage of cell viability for cancer cells and IC<sub>50</sub> values, as depicted in Figure 7. Additionally, morphological changes in cancer cells following exposure to various concentrations of the tested samples are illustrated in the Figure 8. The tested NPs displayed promising dose-dependent profile (you can remove) anticancer effect against skin carcinoma cell lines in agreement with previous reports.<sup>23,72,73</sup> This efficacy was further corroborated by microscopic examination of treated cells, revealing notable alterations in cancer cell morphology such as shrinkage and detachment, particularly at higher concentrations (Figure 8). These findings are consistent with a previous work where *Sea Lavender*-based ZnO NPs exhibited an IC<sub>50</sub> of 409.7 µg/mL against skin cancer cells (A-431), showing major alterations of the cells including extensive shrinkage and detachment.<sup>54</sup> In contrast, LFcQ NPs exhibited negligible activity against A-431 cell lines. These results indicate the highest potency of LFcC NPs against the tested cell lines, demonstrating a significant reduction in cancer cell viability after 72 hours of exposure, reaching cell viability of 0.71% at 1000 µg/mL, with IC<sub>50</sub> value of 263.56 µg/mL compared to the other tested NPs, followed by LZnQ (IC<sub>50</sub> of 481.35 µg/mL). This potency is assumed to be linked to the synergistic effect of iron or zinc elements that form the base of the NPs and the LP phytochemicals, especially the phenolic compounds that are coating the NPs. This is supported by many studies that revealed the potency of Fe, Zn NPs, phenolics, and LP as anticancer agents against several types of cancerous cells due to their cancer cell targeting potentiality and multimodal cancer treatment capacity.<sup>74-77</sup> The possible mechanism of Zn NPs cytotoxicity and genotoxicity against cancer cells was reported to be linked with the intracellular release of soluble zinc ions in the tumor cells due to their acidic microenvironment. This

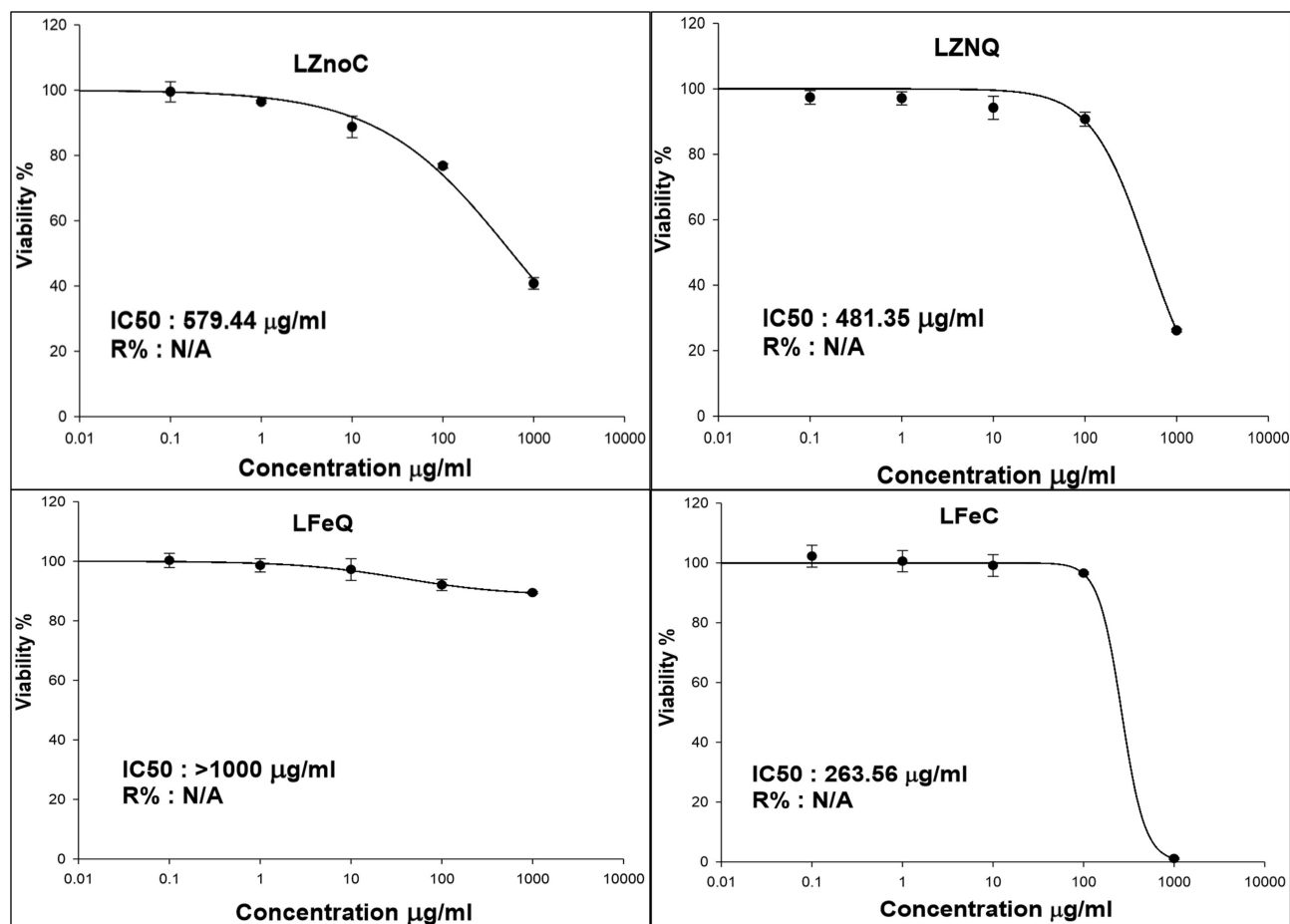


**Figure 7** Anticancer activity of LP corresponding biosynthesized Fe and Zn NPs against A-431 human epidermoid Skin carcinoma. Values are expressed as mean  $\pm$  SD of three independent experiments.

leads to a series of pathways that cause this cytotoxic effect. The first one is the zinc-mediated protein activity disequilibrium, which causes major devastating effects on the cancer cells, such as DNA replication, DNA damage repair, oxidative stress, apoptosis, electron transport chain, cellular homeostasis and membrane permeabilization.<sup>76,78</sup> The second pathway is that the high concentration of the released zinc ions causes the generation of highly reactive oxygen species (ROS), which also increase due to the proinflammatory response of the cells against the NPs and the distinguishing surface property of ZnO NPs that makes them a redox reaction system generating ROS.<sup>79–81</sup> In general, ROS are strong oxidizing agents, so the accumulation of high ROS concentration inside the cell induces oxidative stress due to the misbalance of the oxidative reductive homeostasis of the cell. Eventually, this causes deleterious effects on the proteins (protein denaturation), lipids (lipid peroxidation), and nucleic acids, which ended up with DNA damage and cell death by necrosis and apoptosis.<sup>82–85</sup> Also, several studies reported that the main mechanism of iron oxide NPs in cancer therapy is Fenton reaction-dependent ferroptosis. This happens by the production of iron-mediated oxygen radicals, via the intracellular released iron ions, which causes lipid peroxidation through the Fenton reaction, in addition to triggering the coupling sequence of glutathione and iron redox by the iron-dependent lipid peroxide generator. This causes induction of Fenton reaction-dependent ferroptosis.<sup>77,86</sup> Ferroptosis is an iron-dependent type of nonapoptotic programmed cell death, which is driven by iron-dependent lipid peroxidation and cell metabolism.<sup>87</sup> Furthermore, Phenolic compounds are well known for their anticancer effect through several mechanisms, such as induction of cancerous cellular apoptosis, differentiation, inflammation, angiogenesis, and metastasis through modulation of the redox status under the oxidative stress.<sup>88,89</sup> For example, several phenolic compounds, such as quercetin, apigenin, ellagic acid and resveratrol, were reported to block carcinogenesis through induction of apoptosis, which is triggered via two main

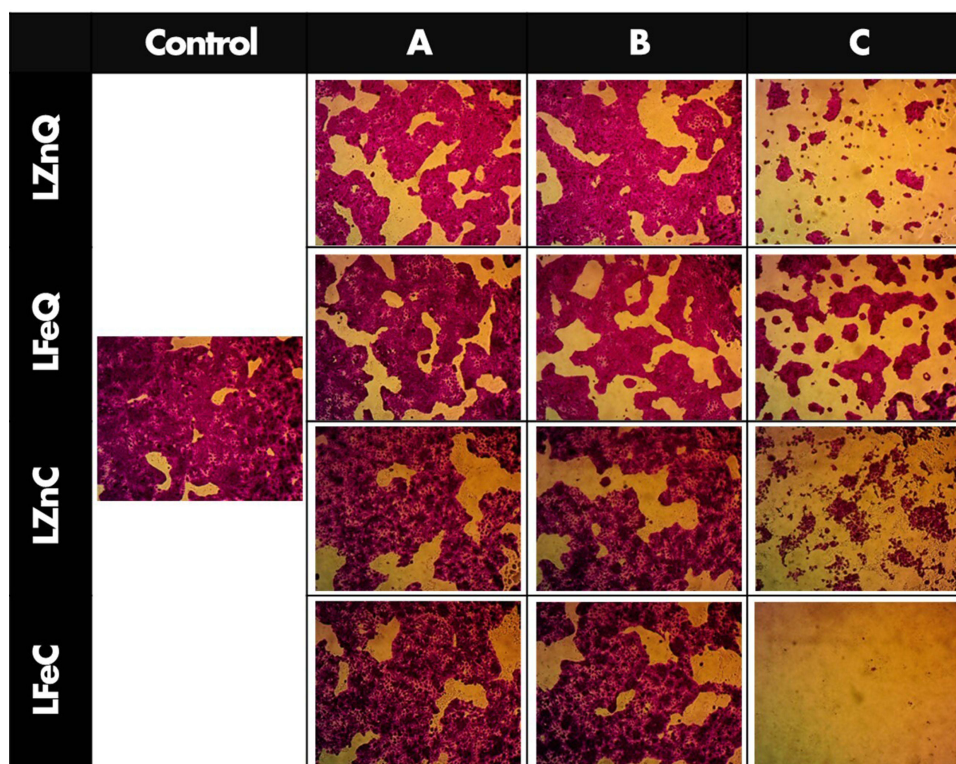


**Figure 8** Morphological changes in A-431 cells after 72 hours of treatment with LP-mediated Fe and Zn NPs; (Control) untreated cancer cells, (A) 0.1 µg/mL, (B) 10 µg/mL, (C) 1000 µg/mL.

pathways: extrinsic and intrinsic.<sup>88</sup> In the extrinsic pathway, activation of cell surface receptors takes place, like tumor necrosis factor-alpha (TNF- $\alpha$ ) that induces caspase-8.

However, in the intrinsic pathway, internal cell signaling is affected through the mitochondria. This is initiated by different categories of mitochondrial proteins, such as the inhibitor of apoptosis proteins (IAPs), small mitochondrial-derived activator of caspases (SMACs), and the B-cell lymphoma-2 protein (Bcl-2), in addition to membrane integrity and polarity.<sup>88,90</sup> In addition, it is previously reported that LP induces a p53-dependent apoptosis, possibly mediated by ROS generation, through intrinsic and extrinsic pathways of cancer cell lines, as it causes activation of caspases, up regulation of Bax and down regulation of Bcl-2.<sup>29</sup> The transcription factor p53 is a key molecule in apoptosis regulation, which suppresses the growth of tumors through regulation of various target genes that possess diverse biological functions, thus protecting against genomic instability and tumorigenesis. This is because it fosters survival by facilitating damage repair, activating checkpoints, and maintaining sustained proliferation blocking and apoptosis.<sup>91</sup>

## Conclusion

This study demonstrated the efficacy of both alcoholic and aqueous extracts of LP as reducing, coating, capping and stabilizing agents in the synthesis of green Fe and Zn NPs for biomedical applications through applying ecofriendly methods that could rival the traditional physical and chemical techniques of Fe and Zn NPs synthesis. In spite of this, the alcoholic extract of LP served better as a coating and capping agent for the biosynthesized Zn and Fe NPs as demonstrated by SEM and EDX. These findings demonstrated a lower tendency of agglomeration in the NPs derived from the alcoholic extract and higher carbon amount than the aqueous extract-based NPs. This was also supported by the TPC and TFC results which revealed their higher phenolic and flavonoid content compared to their aqueous-based counterparts. Beside this, the IR data ensured the successful coating of the NPs with the extracts phytochemicals through showing their functional groups' bands, in addition to confirming the involvement of these phytochemicals in the reduction process of the metal ion during the synthesis process through variation or absence in the intensity of certain

bands in the analyzed NPs compared to their corresponding extracts. As a result of this successful coating, LZnC showed the most pronounced antioxidant effect against DPPH and ABTS radicals, and LFeC revealed the highest potency against A-431 human epidermoid skin carcinoma demonstrating a significant reduction in their viability to 0.71% at 1000 µg/mL after 72 hours of exposure. On the other side, the EDX results suggest the higher potency of the aqueous extract of LP as a reducing agent in the biosynthesis process of Zn and Fe NPs, where the concentrations of Fe and Zn were higher in the aqueous-based NPs compared to their alcoholic counterparts. These findings suggest the suitability of the synthesized green NPs as sustainable anticancer and antioxidant agents that could be promising for other biomedical applications as well. Therefore, we recommend that these bio-formulated green materials undergo extensive chemical and biological studies to determine their mechanism of action, effectiveness, efficacy, and bioavailability in-vivo, beside other kinetics studies. To the best of our knowledge, this is the very first study that reports the biological synthesis of green Zn and Fe NPs utilizing two different types of extracts of LP in general and UAE-wild LP specifically.

## Data Sharing Statement

All the generated and analyzed data within this study are included in this published article.

## Acknowledgment

The authors would like to thank Prof. Dr. Abbas Khaleel and Dr. Fathy M. Hassan from Department of Chemistry, College of Science, UAE University, Al Ain, UAE, for their continuous help and support during the running of this study. Dr. Abdelouahid Samadi thanks the UAEU for an internal Start-up grant 2023 (Grant Code G00004400) for partially supporting this work.

## Author Contributions

All authors made a significant contribution to the work reported, whether that is in the conception, study design, execution, acquisition of data, analysis and interpretation, or in all these areas; took part in drafting, revising or critically reviewing the article; gave final approval of the version to be published; have agreed on the journal to which the article has been submitted; and agree to be accountable for all aspects of the work.

## Disclosure

The authors declare no competing interests in this work.

## References

1. Simões MCF, Sousa JJS, Pais AACC. Skin cancer and new treatment perspectives: a review. *Cancer Lett.* 2015;357(1):8–42. doi:10.1016/j.canlet.2014.11.001
2. Al-Shamsi HO. The state of cancer care in the United Arab Emirates in 2022. *Clin Pract.* 2022;12(6):955–985. doi:10.3390/clinpract12060101
3. Statistics and Research Center. Cancer incidence in United Arab Emirates annual report of the UAE - national cancer registry - 2019; 2019.
4. Apalla Z, Lallas A, Sotiriou E, Lazaridou E, Ioannides D. Epidemiological trends in skin cancer. *Dermatol Pract Concept.* 2017;7(2):1. doi:10.5826/dpc.0702a01
5. Rai M, Ingle AP, Birla S, Yadav A, Dos SCA. Strategic role of selected noble metal nanoparticles in medicine. *Crit Rev Microbiol.* 2015;1–24. doi:10.3109/1040841X.2015.1018131
6. Egorova EM, Kubatiev AA, Schvets VI. *Biological Effects of Metal Nanoparticles.* Springer International Publishing; 2016; doi:10.1007/978-3-319-30906-4
7. Singh J, Dutta T, Kim KH, Rawat M, Samddar P, Kumar P. ‘Green’ synthesis of metals and their oxide nanoparticles: applications for environmental remediation. *J Nanobiotechnol.* 2018;16(1):84. doi:10.1186/s12951-018-0408-4
8. Gebre SH, Sendeku MG. New frontiers in the biosynthesis of metal oxide nanoparticles and their environmental applications: an overview. *SN Appl Sci.* 2019;1(8):1–28. doi:10.1007/s42452-019-0931-4
9. Khatami M, Alijani HQ, Nejad MS, Varma RS. Core@ shell nanoparticles: greener synthesis using natural plant products. *Appl Sci.* 2018;8(3):411. doi:10.3390/app8030411
10. Singh J, Dutta T, Kim KH, Rawat M, Samddar P, Kumar P. ‘Green’ synthesis of metals and their oxide nanoparticles: applications for environmental remediation. *J Nanobiotechnol.* 2018;16(1):1–24. doi:10.1186/s12951-018-0408-4
11. Singh P, Kim YJ, Zhang D, Yang DC. Biological synthesis of nanoparticles from plants and microorganisms. *Trends Biotechnol.* 2016;34(7):588–599. doi:10.1016/j.tibtech.2016.02.006
12. Krishnan V, Mitragotri S. Nanoparticles for topical drug delivery: potential for skin cancer treatment. *Adv Drug Deliv Rev.* 2020;153:87–108. doi:10.1016/j.addr.2020.05.011



13. Satpathy S, Patra A, Ahirwar B, Hussain MD. Process optimization for green synthesis of gold nanoparticles mediated by extract of *Hygrophila spinosa* T. Anders and their biological applications. *Physica E Low Dimens Syst Nanostruct.* 2020;121:113830. doi:10.1016/j.physe.2019.113830
14. Rabiee N, Bagherzadeh M, Kiani M, Ghadiri AM. Rosmarinus officinalis directed palladium nanoparticle synthesis: investigation of potential anti-bacterial, anti-fungal and Mizoroki-Heck catalytic activities. *Adv Powder Tech.* 2020;31(4):1402–1411. doi:10.1016/j.apt.2020.01.024
15. Moradi SZ, Momtaz S, Bayrami Z, Farzaei MH, Abdollahi M. Nanoformulations of herbal extracts in treatment of neurodegenerative disorders. *Front Bioeng Biotechnol.* 2020;8:8. doi:10.3389/fbioe.2020.00238
16. Jain N, Jain P, Rajput D, Patil UK. Green synthesized plant-based silver nanoparticles: therapeutic prospective for anticancer and antiviral activity. *Micro Nano Syst Letters.* 2021;9(1):5. doi:10.1186/s40486-021-00131-6
17. Adewale OB, Egbeyemi KA, Onwuelu JO, et al. Biological synthesis of gold and silver nanoparticles using leaf extracts of *Crassocephalum rubens* and their comparative in vitro antioxidant activities. *Heliyon.* 2020;6(11):e05501. doi:10.1016/j.heliyon.2020.e05501
18. Abbasi BA, Iqbal J, Mahmood T, Qyum A, Kanwal S. Biofabrication of iron oxide nanoparticles by leaf extract of *Rhamnus virgata*: characterization and evaluation of cytotoxic, antimicrobial and antioxidant potentials. *Appl Organomet Chem.* 2019;33(7):e4947. doi:10.1002/aoc.4947
19. Herlekar M, Barve S, Kumar R. Plant-mediated green synthesis of iron nanoparticles. *J Nanopart.* 2014;2014:1–9. doi:10.1155/2014/140614
20. Ebrahiminezhad A, Zare-Hoseinabadi A, Sarmah AK, Taghizadeh S, Ghasemi Y, Berenjian A. Plant-mediated synthesis and applications of iron nanoparticles. *Mol Biotechnol.* 2018;60(2):154–168. doi:10.1007/s12033-017-0053-4
21. Rana A, Yadav K, Jagadevan S. A comprehensive review on green synthesis of nature-inspired metal nanoparticles: mechanism, application and toxicity. *J Clean Prod.* 2020;272:122880. doi:10.1016/j.jclepro.2020.122880
22. Hameed S, Iqbal J, Ali M, et al. Green synthesis of zinc nanoparticles through plant extracts: establishing a novel era in cancer theranostics. *Mater Res Express.* 2019;6(10):102005. doi:10.1088/2053-1591/ab40df
23. Naiel B, Fawzy M, Halmy MWA, Mahmoud AED. Green synthesis of zinc oxide nanoparticles using Sea Lavender (*Limonium pruinatum* L. Chaz.) extract: characterization, evaluation of anti-skin cancer, antimicrobial and antioxidant potentials. *Sci Rep.* 2022;12(1):20370. doi:10.1038/s41598-022-24805-2
24. Feng RY, Chen W, Guang LX, et al. Epirubicin-loaded superparamagnetic iron-oxide nanoparticles for transdermal delivery: cancer therapy by circumventing the skin barrier. *Small.* 2015;11(2):239–247. doi:10.1002/sml.201400775
25. Amatya R, Kim D, Min KA, Shin MC. Iron oxide nanoparticles-loaded hydrogels for effective topical photothermal treatment of skin cancer. *J Pharm Investig.* 2022;52(6):775–785. doi:10.1007/s40005-022-00593-9
26. Khasawneh MA, Elwy HM, Hamza AA, Fawzi NM, Hassan AH. Antioxidant, anti-lipoxygenase and cytotoxic activity of *Leptadenia pyrotechnica* (Forssk.) decne polyphenolic constituents. *Molecules.* 2011;16(9):7510–7521. doi:10.3390/molecules16097510
27. Preet R, Gupta RC, Pradhan SK. Chromatographic determination of  $\beta$ -sitosterol, lupeol, and oleanolic acid in *Leptadenia pyrotechnica* (Forsk.) decne.—A botanical source of the ayurvedic drug Jivanti. *JPC-J Planar Chromat-Mod TLC.* 2018;31(2):150–154. doi:10.1556/1006.2018.31.2.9
28. Youssef Moustafa AM, Khodair AI, Saleh MA. Isolation, structural elucidation of flavonoid constituents from *Leptadenia pyrotechnica* and evaluation of their toxicity and antitumor activity. *Pharm Biol.* 2009;47(6):539–552. doi:10.1080/13880200902875065
29. Khasawneh MA, Koch A, Elwy HM, Hamza AA, Schneider-Stock R. *Leptadenia pyrotechnica* induces p53-dependent apoptosis in colon cancer cells. *Nat Prod Chem Res.* 2015;3:1–8.
30. Abbas A, Naqvi SAR, Rasool MH, Noureen A, Mubarak MS, Tareen RB. Phytochemical analysis, antioxidant and antimicrobial screening of seriphidium oliverianum plant extracts. *Dose-Response.* 2021;19(1):155932582110047. doi:10.1177/15593258211004739
31. Zhan Q, Han J, Sheng L. Iron nanoparticles green-formulated by *Coriandrum sativum* leaf aqueous extract: investigation of its anti-liver-cancer effects. *Arch Med Sci.* 2013;9(3):581–583. doi:10.5114/aoms.2013.35020
32. Ashraf H, Meer B, Iqbal J, et al. Comparative evaluation of chemically and green synthesized zinc oxide nanoparticles: their in vitro antioxidant, antimicrobial, cytotoxic and anticancer potential towards HepG2 cell line. *J Nanostruct Chem.* 2023;13:1–19.
33. Kambale EK, Katemo FM, Quetin-Leclercq J, Memvanga PB, Beloqui A. “Green”-synthesized zinc oxide nanoparticles and plant extracts: a comparison between synthesis processes and antihyperglycemic activity. *Int J Pharm.* 2023;635:122715. doi:10.1016/j.ijpharm.2023.122715
34. Stéphane FFY, Jules BKJ, Batiha GES, Ali I, Bruno LN. Extraction of bioactive compounds from medicinal plants and herbs. *Nat Med Plants.* 2021;2021:1–39.
35. Gates-Rector S, Blanton T. The powder diffraction file: a quality materials characterization database. *Powder Diffr.* 2019;34(4):352–360. doi:10.1017/S0885715619000812
36. Mourdikoudis S, Pallares RM, Thanh NTK. Characterization techniques for nanoparticles: comparison and complementarity upon studying nanoparticle properties. *Nanoscale.* 2018;10(27):12871–12934. doi:10.1039/C8NR02278J
37. Saboo S, Tapadiya R, Khadabadi S, Deokate U. In vitro antioxidant activity and total phenolic, flavonoid contents of the crude extracts of *Pterospermum acerifolium* wild leaves (Sterculiaceae). *J Chem Pharm Res.* 2010;2(3):417–423.
38. Swain T, Hillis WE. The phenolic constituents of *Prunus domestica*. I.—The quantitative analysis of phenolic constituents. *J Sci Food Agric.* 1959;10(1):63–68. doi:10.1002/jsfa.2740100110
39. Mabry T, Markham KR, Thomas MB. *The Systematic Identification of Flavonoids*. Springer Science & Business Media; 2012.
40. El-Hawary EA, Zayed A, Laub A, Modolo LV, Wessjohann L, Farag MA. How does LC/MS compare to UV in coffee authentication and determination of antioxidant effects? Brazilian and Middle Eastern coffee as case studies. *Antioxidants.* 2022;11(1):131. doi:10.3390/antiox11010131
41. Üstün E, Önbaşı SC, Çelik SK, Ayvaz MÇ, Şahin N. Green synthesis of iron oxide nanoparticles by using *Ficus carica* leaf extract and its antioxidant activity. *Biointerface Res Appl Chem.* 2022;2021(12):2108–2116.
42. Guha G, Rajkumar V, Kumar RA, Mathew L. Antioxidant activity of *Lawsonia inermis* extracts inhibits chromium (VI)-induced cellular and DNA toxicity. *Evidence-Based Complem Alternat Med.* 2011;2011. doi:10.1093/ecam/nep205
43. Kim MJ, Kim DH, Kwak HS, Yu IS, Um MY. Protective effect of *Chrysanthemum boreale* flower extracts against A2E-induced retinal damage in ARPE-19 cell. *Antioxidants.* 2022;11(4):669. doi:10.3390/antiox11040669
44. Rajurkar NS, Hande SM. Estimation of phytochemical content and antioxidant activity of some selected traditional Indian medicinal plants. *Indian J Pharm Sci.* 2011;73(2):146. doi:10.4103/0250-474X.91574

45. Skehan P, Storeng R, Scudiero D, et al. New colorimetric cytotoxicity assay for anticancer-drug screening. *JNCI*. 1990;82(13):1107–1112. doi:10.1093/jnci/82.13.1107
46. Allam RM, Al-Abd AM, Khedr A, et al. Fingolimod interrupts the cross talk between estrogen metabolism and sphingolipid metabolism within prostate cancer cells. *Toxicol Lett*. 2018;291:77–85. doi:10.1016/j.toxlet.2018.04.008
47. Ahmida A, Mahdavi B, Zaker F, et al. Chemical characterization and anti-hemolytic anemia potentials of tin nanoparticles synthesized by a green approach for bioremediation applications. *Appl Organomet Chem*. 2020;34(3). doi:10.1002/aoc.5433
48. Baghayeri M, Mahdavi B, Hosseinpour-Mohsen Abadi Z, Farhadi S. Green synthesis of silver nanoparticles using water extract of *Salvia leriifolia*: antibacterial studies and applications as catalysts in the electrochemical detection of nitrite. *Appl Organomet Chem*. 2018;32(2). doi:10.1002/aoc.4057
49. Mahdavi B, Saneei S, Qorbani M, et al. *Ziziphora clinopodioides* Lam leaves aqueous extract mediated synthesis of zinc nanoparticles and their antibacterial, antifungal, cytotoxicity, antioxidant, and cutaneous wound healing properties under in vitro and in vivo conditions. *Appl Organomet Chem*. 2019;33(11). doi:10.1002/aoc.5164
50. Mahdavi B, Paydarfarid S, Zangeneh MM, Goorani S, Seydi N, Zangeneh A. Assessment of antioxidant, cytotoxicity, antibacterial, antifungal, and cutaneous wound healing activities of green synthesized manganese nanoparticles using *Ziziphora clinopodioides* Lam leaves under in vitro and in vivo condition. *Appl Organomet Chem*. 2020;34(1). doi:10.1002/aoc.5248
51. Ibraheem F, Aziz MH, Fatima M, Shaheen F, Ali SM, Huang Q. In vitro cytotoxicity, MMP and ROS activity of green synthesized nickel oxide nanoparticles using extract of *Terminalia chebula* against MCF-7 cells. *Mater Lett*. 2019;234:129–133. doi:10.1016/j.matlet.2018.09.075
52. Iqbal J, Abbasi BA, Mahmood T, Hameed S, Munir A, Kanwal S. Green synthesis and characterizations of nickel oxide nanoparticles using leaf extract of *Rhamnus virgata* and their potential biological applications. *Appl Organomet Chem*. 2019;33(8). doi:10.1002/aoc.4950
53. Karmakar S. Particle size distribution and zeta potential based on dynamic light scattering: techniques to characterize stability and surface charge distribution of charged colloids. *Recent Trends Mater Phys Chem*. 2019;28:117–159.
54. Chauhan S, Upadhyay LSB. Biosynthesis of iron oxide nanoparticles using plant derivatives of *Lawsonia inermis* (Henna) and its surface modification for biomedical application. *Nanotechnol Environ Eng*. 2019;4:1–10. doi:10.1007/s41204-019-0055-5
55. Sri Sindhura K, V. PTNVK, Panner Selvam P, Hussain OM. Synthesis, characterization and evaluation of effect of phyto-genic zinc nanoparticles on soil exo-enzymes. *Appl Nanosci*. 2014;4(7):819–827. doi:10.1007/s13204-013-0263-4
56. Bradley M. FTIR basic organic functional group reference chart. *Thermo Fisher Scientific*. 2015;2015:21.
57. Afrouz M, Ahmadi-Nouraldin F, Elias SG, Alebrahim MT, Tseng TM, Zahedian H. Green synthesis of spermine coated iron nanoparticles and its effect on biochemical properties of *Rosmarinus officinalis*. *Sci Rep*. 2023;13(1):775. doi:10.1038/s41598-023-27844-5
58. Metwally AA, Abdel-Hady ANAA, Haridy MAM, Ebnalwaled K, Saied AA, Soliman AS. Wound healing properties of green (using *Lawsonia inermis* leaf extract) and chemically synthesized ZnO nanoparticles in albino rats. *Environ Sci Pollut Res*. 2022;2022:1–13.
59. Kinayyigit S. Role of phenols and phenol derivatives in the synthesis of nanoparticles. *Reducing Agents in Colloidal Nanoparticle Synthesis*. 2021. 73–96.
60. Wu D, Zhou J, Creyer MN, et al. Phenolic-enabled nanotechnology: versatile particle engineering for biomedicine. *Chem Soc Rev*. 2021;50(7):4432–4483. doi:10.1039/d0cs00908c
61. Amini SM, Akbari A. Metal nanoparticles synthesis through natural phenolic acids. *IET Nanobiotechnol*. 2019;13(8):771–777. doi:10.1049/iet-nbt.2018.5386
62. Rahman MM, Rahaman MS, Islam MR, et al. Role of phenolic compounds in human disease: current knowledge and future prospects. *Molecules*. 2021;27(1):233. doi:10.3390/molecules27010233
63. Sujarwo W, Keim AP. Chapter 27-Spondias pinnata (L. f.) Kurz.(Anacardiaceae): profiles and applications to diabetes. *Bioactive Food as Dietary Interventions for Diabetes (Second Edition)*. Academic Press, London; 2019. 395–405.
64. Floegel A, Kim DO, Chung SJ, Koo SI, Chun OK. Comparison of ABTS/DPPH assays to measure antioxidant capacity in popular antioxidant-rich US foods. *J Food Compos Anal*. 2011;24(7):1043–1048. doi:10.1016/j.jfca.2011.01.008
65. Foti MC, Daquino C, Geraci C. Electron-transfer reaction of cinnamic acids and their methyl esters with the DPPH• radical in alcoholic solutions. *J Org Chem*. 2004;69(7):2309–2314. doi:10.1021/jo035758q
66. Xiao Z, Wang Y, Wang J, Li P, Ma F. Structure-antioxidant capacity relationship of dihydrochalcone compounds in *Malus*. *Food Chem*. 2019;275:354–360. doi:10.1016/j.foodchem.2018.09.135
67. Platzer M, Kiese S, Herfellner T, Schweiggert-Weisz U, Miesbauer O, Eisner P. Common trends and differences in antioxidant activity analysis of phenolic substances using single electron transfer based assays. *Molecules*. 2021;26(5):1244. doi:10.3390/molecules26051244
68. Afzal MA, Javed M, Aroob S, et al. The biogenic synthesis of bimetallic Ag/ZnO nanoparticles: a multifunctional approach for methyl violet photocatalytic degradation and the assessment of antibacterial, antioxidant, and cytotoxicity properties. *Nanomaterials*. 2023;13(14):2079. doi:10.3390/nano13142079
69. Firoozi S, Jamzad M, Yari M. Biologically synthesized silver nanoparticles by aqueous extract of *Satureja intermedia* CA Mey and the evaluation of total phenolic and flavonoid contents and antioxidant activity. *J Nanostructure Chem*. 2016;6:357–364. doi:10.1007/s40097-016-0207-0
70. Subramanian R, Subramaniyan P, Raj V. Antioxidant activity of the stem bark of *Shorea roxburghii* and its silver reducing power. *Springerplus*. 2013;2:1–11. doi:10.1186/2193-1801-2-28
71. Ahmad N, Sharma S. Green synthesis of silver nanoparticles using extracts of *Ananas comosus*. *Green Sustain Chem*. 2012;02(04):141–147. doi:10.4236/gsc.2012.24020
72. Saranya S, Vijayanarai K, Pavithra S, Raihana N, Kumanan K. In vitro cytotoxicity of zinc oxide, iron oxide and copper nanopowders prepared by green synthesis. *Toxicol Rep*. 2017;4:427–430. doi:10.1016/j.toxrep.2017.07.005
73. Chelladurai M, Sahadevan R, Margavelu G, et al. Anti-skin cancer activity of *Alpinia calcarata* ZnO nanoparticles: characterization and potential antimicrobial effects. *J Drug Deliv Sci Technol*. 2021;61:102180. doi:10.1016/j.jddst.2020.102180
74. Ma H, Wang C, Li X, Sui D, Xu S. Efficiency of the green formulated iron nanoparticles as a new tool in lung cancer therapy. *Arabian J Chem*. 2023;16(8):104928. doi:10.1016/j.arabjc.2023.104928
75. Majeed S, Danish M, Bin IMH, Ansari MT, Ibrahim MNM. Anticancer and apoptotic activity of biologically synthesized zinc oxide nanoparticles against human colon cancer HCT-116 cell line-in vitro study. *Sustain Chem Pharm*. 2019;14:100179. doi:10.1016/j.scp.2019.100179
76. Bisht G, Rayamajhi S. ZnO nanoparticles: a promising anticancer agent. *Nanobiomedicine*. 2016;3:9. doi:10.5772/63437

77. Lin L, Chen H, Zhao R, Zhu M, Nie G. Nanomedicine targets iron metabolism for cancer therapy. *Cancer Sci.* 2022;113(3):828–837. doi:10.1111/cas.15250
78. Shen C, James SA, de Jonge MD, Turney TW, Wright PFA, Feltis BN. Relating cytotoxicity, zinc ions, and reactive oxygen in ZnO nanoparticle-exposed human immune cells. *Toxicol Sci.* 2013;136(1):120–130. doi:10.1093/toxsci/kft187
79. Song W, Zhang J, Guo J, et al. Role of the dissolved zinc ion and reactive oxygen species in cytotoxicity of ZnO nanoparticles. *Toxicol Lett.* 2010;199(3):389–397. doi:10.1016/j.toxlet.2010.10.003
80. Rasmussen JW, Martinez E, Louka P, Wingett DG. Zinc oxide nanoparticles for selective destruction of tumor cells and potential for drug delivery applications. *Expert Opin Drug Deliv.* 2010;7(9):1063–1077. doi:10.1517/17425247.2010.502560
81. Wilson M. Interactions between ultrafine particles and transition metals in vivo and in vitro. *Toxicol Appl Pharmacol.* 2002;184(3):172–179. doi:10.1006/taap.2002.9501
82. Dhawan DK, Chadha VD. Zinc: a promising agent in dietary chemoprevention of cancer. *Indian J Med Res.* 2010;132(6):676–682.
83. Ng KW, Khoo SPK, Heng BC, et al. The role of the tumor suppressor p53 pathway in the cellular DNA damage response to zinc oxide nanoparticles. *Biomaterials.* 2011;32(32):8218–8225. doi:10.1016/j.biomaterials.2011.07.036
84. Valko M, Rhodes CJ, Moncol J, Izakovic M, Mazur M. Free radicals, metals and antioxidants in oxidative stress-induced cancer. *Chem Biol Interact.* 2006;160(1):1–40. doi:10.1016/j.cbi.2005.12.009
85. Manke A, Wang L, Rojanasakul Y. Mechanisms of nanoparticle-induced oxidative stress and toxicity. *Biomed Res Int.* 2013;2013:1–15. doi:10.1155/2013/942916
86. Wen J, Chen H, Ren Z, Zhang P, Chen J, Jiang S. Ultrasmall iron oxide nanoparticles induced ferroptosis via Beclin1/ATG5-dependent autophagy pathway. *Nano Conver.* 2021;8:1–15. doi:10.1186/s40580-021-00260-z
87. Dixon SJ, Stockwell BR. The hallmarks of ferroptosis. *Annu Rev Cancer Biol.* 2019;3(1):35–54. doi:10.1146/annurev-cancerbio-030518-055844
88. Basli A, Belkacem N, Amrani I. Health benefits of phenolic compounds against cancers. *Phenolic Compounds-Biol Act.* 2017;8:193–210.
89. Wahle KWJ, Brown I, Rotondo D, Heys SD. Plant phenolics in the prevention and treatment of cancer. *Bio-Farms Nutraceut.* 2010;2010:36–51.
90. Wang L, Du F, Wang X. TNF- $\alpha$  induces two distinct caspase-8 activation pathways. *Cell.* 2008;133(4):693–703. doi:10.1016/j.cell.2008.03.036
91. Lavin MF, Gueven N. The complexity of p53 stabilization and activation. *Cell Death Differ.* 2006;13(6):941–950. doi:10.1038/sj.cdd.4401925

International Journal of Nanomedicine

Dovepress

## Publish your work in this journal

The International Journal of Nanomedicine is an international, peer-reviewed journal focusing on the application of nanotechnology in diagnostics, therapeutics, and drug delivery systems throughout the biomedical field. This journal is indexed on PubMed Central, MedLine, CAS, SciSearch<sup>®</sup>, Current Contents<sup>®</sup>/Clinical Medicine, Journal Citation Reports/Science Edition, EMBase, Scopus and the Elsevier Bibliographic databases. The manuscript management system is completely online and includes a very quick and fair peer-review system, which is all easy to use. Visit <http://www.dovepress.com/testimonials.php> to read real quotes from published authors.

Submit your manuscript here: <https://www.dovepress.com/international-journal-of-nanomedicine-journal>